Dynamics of a multi-pulse excited rotating beam system

Hongliang Hua (huahl123@126.com)
Changzhou Institute of Technology https://orcid.org/0000-0002-4933-1682

Short Report

Keywords: rotating beam, multi-pulse excitation, periodic motion, rigid-flexible coupling dynamics, machine gun system

Posted Date: October 27th, 2022

DOI: https://doi.org/10.21203/rs.3.rs-2204011/v1 applied sciences

MDPI

Article

Dynamics of a multi-pulse excited rotating beam system

Hong-liang Hua

[1] School of Aeronautics and Mechanical Engineering, Changzhou Institute of Technology, Changzhou, Jiangsu 213032, China; huahl123@126.com

Abstract: The periodic motion characteristic is crucial for the firing accuracy of the machine gun system. In this study, a demonstrated machine gun system is simplified as a rotating beam system to study its periodic motion characteristic under a multi-pulsed excitation. Unlike the previously rotating beam model, the beam axis and the rotation center are non-collinear. The nonlinear coupled dynamic model of the system is derived by Rayleigh-Ritz method and Lagrange equation, and the dynamic responses are analyzed using Runge-Kutta method. Based on the computed responses, the effect of rotating radius, beam length, torsional stiffness and damping on system dynamic behavior are analyzed and discussed. Results reveal that increasing the rotating radius and beam length could affect the periodic motion of the system gradually. Increasing the torsional stiffness could enhance the periodic motion characteristic of the rotating beam system. The quasi-periodic motion characterized of the system could be dominated by matching the torsional damping.

Keywords: rotating beam; multi-pulse excitation; periodic motion; rigid-flexible coupling dynamics; machine gun system

Citation: Lastname, F.; Lastname, F.; Lastname, F. Title. *Appl. Sci.* **2022**, *12*, x. https://doi.org/10.3390/xxxxx

Academic Editor: Firstname Lastname

Received: date
Accepted: date
Published: date

1. Introduction

Periodic vibration characteristic is one of the major factors of the firing accuracy of the machine gun system [1-3]. Due to the elastic deformation of the machine gun system during the firing process, the initial conditions of the bullet will be directly affected by the muzzle vibration [4]. In other words, the final bullet dispersion (firing accuracy) depends on the muzzle dynamic behavior directly. A feasible way to improve the firing accuracy is to reduce the muzzle vibration [5] or set the system parameters to ensure the muzzle vibrates periodically [6]. In our study, the demonstrated machine gun system is simplified as a rotating beam system, as illustrated in Fig. 2, to study the effects of system parameters on its periodic motion characteristics.

In previous literatures, the dynamics of the rotating beam system has been studied extensively. The topic has covered rotating tapered beam [7], rotating composite beam[8], vibration control [9], rotating beam with a tip mass. This model is quite different from the previous literatures and the main differences are as follows: (1) The beam axis and the rotation center are non-collinear. In previous literature, the beam axis is considered collinear to the rotation center [10, 11]. Since their potential engineering background may be helicopter rotor blades [12], aircraft engine [13], robotic manipulators, and turbine blades [14, 15]. For the machine gun system, considering the rotating beam with an axis eccentricity is more appropriate. (2) The rigid body motion is small. Therefore, the dynamic stiffening effect [16] is not considered here. (3) The rotating beam system is subjected to the multi-pulse excitation to simulate the dynamic behavior of the machine gun system which fires continuously. The torsional stiffness and damping effect between the hub and ground are considered. (4) This study mainly focusses on the effects of system parameters on the periodic motion characteristic of the beam's tip. Since the firing accuracy of the machine gun system depends directly on the muzzle periodic motion.

The rest of this paper is organized as follows: in Section 2 the nonlinear coupled motion equations of the rotating beam system is derived using the Rayleigh-Ritz method and the Lagrange equation. The post processing formulation of the beam tip responses is given. In section 3, the Runge-Kutta method is used to analyze the dynamic responses of the system. Based on the responses, the nonlinear coupled motion equations are validated by comparing the present results with those simulated by ADAMS software. Finally, the effects of rotating radius, beam length, torsional stiffness and damping on system dynamic behavior are discussed.

2. System energy description

According to the structural deformation characteristic of the machine gun system during the firing process (Fig. 1), the machine gun system is simplified as a rotating beam system approximately, as shown in Fig. 2. The flexible beam is fixed to the rigid rotating hub, and the beam rotates with the hub in the vertical plane. Therefore, the gravity effect is considered here. The coordinate system O_0-X_0Y_0 is the inertia coordinate system, while the O_1-X_1Y_1 is the relative coordinate system which fixed to the flexible beam. The flexible beam has a Young's modulus E, area moment of inertia I, density ρ, cross-sectional area A and length L. The transverse deflection of the flexible beam in the O_1-X_1Y_1 is described by $w(x,t)$. The hub radius and rotation angle are denoted by r and θ, respectively. The torsional stiffness k and damping c of the revolute joint between the rotating hub and the base are considered to simulate the tripod torsional deformation characteristic.

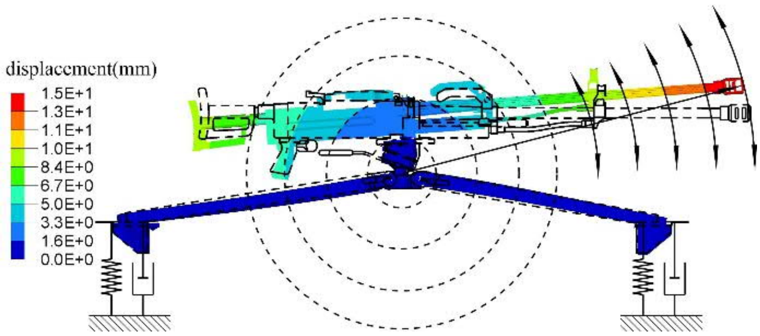

Fig. 1 Structural deformation of a machine gun system during firing [17].

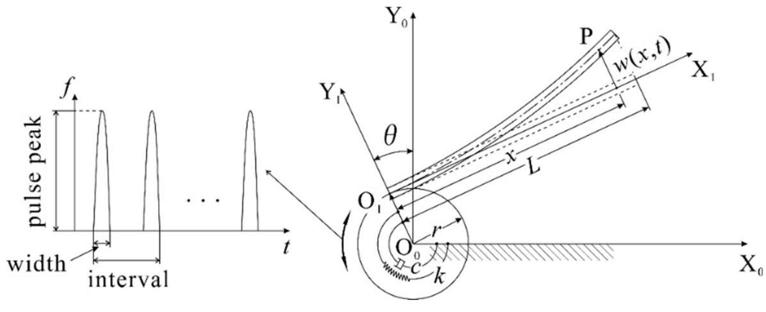

Fig. 2 Rotating beam model.

2.1. Energy expressions of the rotating beam system

It should be noted that the angular displacement and velocity of the machine gun body during the firing process is quite small [18-20], therefore the longitudinal deformation of the flexible beam is not considered here. Thus, the displacement of an arbitrary point P in the flexible beam is

$$\mathbf{R}_P = \left(x\cos\theta - \left(w+r\right)\sin\theta\right)\mathbf{i} + \left(x\sin\theta + \left(w+r\right)\cos\theta\right)\mathbf{j} \tag{1}$$

where, $\mathbf{i}$ and $\mathbf{j}$ are the unit vector in the directions of X_0 and Y_0 axes.

The velocity vector of the point P could be obtained by taking the differentiation of Eq. (1) with respect to time t as

$$\dot{\mathbf{R}}_P = \left(-x\dot{\theta}\sin\theta - \dot{w}\sin\theta - \left(w+r\right)\dot{\theta}\cos\theta\right)\mathbf{i} + \left(x\dot{\theta}\cos\theta + \dot{w}\cos\theta - \left(w+r\right)\dot{\theta}\sin\theta\right)\mathbf{j} \tag{2}$$

where dot denotes the derivation with respect to time.

The kinetic energy of the rotating beam system is given by

$$T = \frac{1}{2}J\dot{\theta}^2 + \frac{1}{2}\rho A\int_0^L \dot{\mathbf{R}}_P \cdot \dot{\mathbf{R}}_P dx \tag{3}$$

where the first term denotes the rotational kinetic energy of the hub; the second term denotes the kinetic energy of the flexible beam; J is the moment of inertia of the rigid hub.

Consider $\theta = 0$ and $w = 0$ as the zero point of the system potential energy, the potential energy of the system is given by [21]

$$U = \frac{1}{2}k\theta^2 + \frac{1}{2}EI\int_0^L w''^2 dx + \rho Ag\int_0^L \left(\mathbf{R}_P \cdot \mathbf{j} - r\right)dx \tag{4}$$

where the three terms express the rotational potential energy of the hub, the strain energy of flexible beam and the gravitational potential energy. The prime denotes the derivation with respect to x coordinate.

2.2. Method of solution

In this section, the Rayleigh-Ritz method is used to derive the motion equations of the system. According to the Rayleigh-Ritz method, the transverse deflection of the beam $w\left(x,t\right)$ is discretized in the form as

$$w\left(x,t\right) = \mathbf{N}\left(x\right)\mathbf{q}\left(t\right) \tag{5}$$

where

$$\mathbf{N}\left(x\right) = \left[N_1\left(x\right), N_2\left(x\right), \ldots, N_n\left(x\right)\right] \tag{6}$$

$$\mathbf{q}\left(t\right) = \left[q_1\left(t\right), q_2\left(t\right), \ldots, q_n\left(t\right)\right]^T \tag{7}$$

where $N_i\left(x\right)$, $i = 1, 2, \ldots, n$ are the basis functions, which satisfys all (or part of) the boundary conditions; $q_i\left(t\right)$ are the time-dependent generalized coordinates in the O_1-X_1Y_1; n denotes the number of the basic functions.

By substituting Eq. (5) into Eqs. (3) and (4), one could obtain the discretized kinetic energy and potential energy forms as

$$T = \frac{1}{2}J\dot{\theta}^2 + \frac{1}{6}\rho AL\dot{\theta}^2\left(L^2 + 3r^2\right) + \frac{1}{2}\dot{\mathbf{q}}^T\mathbf{m}_1\dot{\mathbf{q}} + \dot{\theta}\dot{\mathbf{q}}^T\mathbf{f}_1 + \frac{1}{2}\dot{\theta}^2\mathbf{q}^T\mathbf{m}_1\mathbf{q} + \dot{\theta}^2\mathbf{q}^T\mathbf{f}_2 \tag{8}$$

$$U = \frac{1}{2}k\theta^2 + \frac{1}{2}\mathbf{q}^T\mathbf{k}_1\mathbf{q} + \frac{1}{2}\rho AL^2 g\sin\theta + \cos\theta\mathbf{q}^T\mathbf{f}_3 + \rho AgL\left(r\cos\theta - r\right) \tag{9}$$

where

$$\mathbf{m}_1 = \rho A\int_0^L \left(\mathbf{N}^T\mathbf{N}\right)dx,\ \mathbf{k}_1 = EI\int_0^L \mathbf{N}''^T\mathbf{N}''dx \tag{10, 11}$$

$$\mathbf{f}_1 = \rho A\int_0^L \left(x\mathbf{N}^T\right)dx,\ \mathbf{f}_2 = r\rho A\int_0^L \left(\mathbf{N}^T\right)dx \tag{12, 13}$$

$$\mathbf{f}_3 = \rho Ag\int_0^L \left(\mathbf{N}^T\right)dx \tag{14}$$

To derive the motion equations of the system, the Lagrange equations is adopted here and the general form could be given by [22]

$$\frac{d}{dt}\left(\frac{\partial T}{\partial \dot{\mathbf{q}}^T}\right) - \frac{\partial T}{\partial \mathbf{q}^T} + \frac{\partial U}{\partial \mathbf{q}^T} = \mathbf{0},\ \frac{d}{dt}\left(\frac{\partial T}{\partial \dot{\theta}}\right) - \frac{\partial T}{\partial \theta} + \frac{\partial U}{\partial \theta} = f \tag{15, 16}$$

where f denotes the generalized torque excitation as displayed in Fig. 2.

Once substituting Eqs. (8) and (9) into Eqs. (15) and (16), the nonlinear coupled motion equations could be obtained as

$$\left(J+\frac{1}{3}\rho AL\left(L^2+3r^2\right)+\mathbf{q}^T\mathbf{m}_1\mathbf{q}+2\mathbf{f}_2^T\mathbf{q}\right)\ddot{\theta}+\left(c+2\mathbf{q}^T\mathbf{m}_1\dot{\mathbf{q}}+2\mathbf{f}_2^T\dot{\mathbf{q}}\right)\dot{\theta}+$$
$$k\theta+\mathbf{f}_1^T\ddot{\mathbf{q}}-\sin\theta\mathbf{f}_3^T\mathbf{q}=\rho ALg\left(r\sin\theta-\frac{1}{2}L\cos\theta\right)+f \tag{17}$$

$$\mathbf{m}_1\ddot{\mathbf{q}}+\left(\mathbf{k}_1-\dot{\theta}^2\mathbf{m}_1\right)\mathbf{q}+\mathbf{f}_1\ddot{\theta}-\mathbf{f}_2\dot{\theta}^2=-\cos\theta\mathbf{f}_3 \tag{18}$$

To consider the structural damping effect of the flexible beam, the Rayleigh damping model [23] is adopted and given by

$$\mathbf{c}=\alpha\mathbf{m}_1+\beta\mathbf{k}_1 \tag{19}$$

where, α and β are two damping coefficients.

According to Eq. (19), the Eq. (18) is modified as

$$\mathbf{m}_1\ddot{\mathbf{q}}+\mathbf{c}\dot{\mathbf{q}}+\left(\mathbf{k}_1-\dot{\theta}^2\mathbf{m}_1\right)\mathbf{q}+\mathbf{f}_1\ddot{\theta}-\mathbf{f}_2\dot{\theta}^2=-\cos\theta\mathbf{f}_3 \tag{20}$$

The dynamic responses of the system ($\theta(t)$, $q_i(t)$, $i=1,2,\ldots,n$) could be obtained by solving the nonlinear coupled Eqs. (17) and (20) simultaneously using the time integration method. In our study, the Runge-Kutta method [24] is used.

By introducing $x=L$, $w=\sum_{i=1}^{n}q_i(t)$ to Eqs. (1) and (2), one obtains the beam tip displacement and velocity vector in the inertia system as

$$\mathbf{R}_{tip}=\left(L\cos\theta(t)-\left(\sum_{i=1}^{n}q_i(t)+r\right)\sin\theta(t)\right)\mathbf{i}+$$
$$\left(L\sin\theta(t)+\left(\sum_{i=1}^{n}q_i(t)+r\right)\cos\theta(t)\right)\mathbf{j} \tag{21}$$

$$\dot{\mathbf{R}}_{tip}=\begin{pmatrix}-L\dot{\theta}(t)\sin\theta(t)-\sum_{i=1}^{n}\dot{q}_i(t)\sin\theta(t)-\\ \left(\sum_{i=1}^{n}q_i(t)+r\right)\dot{\theta}(t)\cos\theta(t)\end{pmatrix}\mathbf{i}+$$
$$\begin{pmatrix}L\dot{\theta}(t)\cos\theta(t)+\sum_{i=1}^{n}\dot{q}_i(t)\cos\theta(t)-\\ \left(\sum_{i=1}^{n}q_i(t)+r\right)\dot{\theta}(t)\sin\theta(t)\end{pmatrix}\mathbf{j} \tag{22}$$

The beam tip response in the Y_0 axis direction could be obtained by

$$\mathbf{R}_{tip,y}=\mathbf{R}_{tip}\cdot\mathbf{j},\ \dot{\mathbf{R}}_{tip,y}=\dot{\mathbf{R}}_{tip}\cdot\mathbf{j} \tag{23}$$

3. Results and discussion

In this section, the effects of rotating radius, beam length, torsional stiffness and damping on system dynamic behavior are analyzed and discussed based on the computed response. Since these parameters are adjustable from the point of structural design. Study the effects of the above parameters could provide a reference for the engineering application.

3.1. Validation

In this subsection, the dynamic model established in section 2 is validated by comparing the results with the famous dynamic analysis software ADAMS. In following, if not specified otherwise, the system parameters are E=2e11N/m², I =1.33e-8m⁴, ρ

$=7900\text{kg/m}^3$, $A=4\text{e-}4\text{m}^2$, $J=0.1225\text{kg}\cdot\text{m}^2$, $L=1\text{m}$, $r=0.1\text{m}$, $c=10\text{N}\cdot\text{m}\cdot\text{rad/s}$, $k=5000\text{N}\cdot\text{m/rad}$.

In simulation, a half-sine torque excitation is applied to the hub as

$$f=50\sin\left(50\pi t\right)\quad for\ 0\le t\le 0.01 \tag{24}$$

After the excitation disappears, the system vibrates freely. The dynamic responses are compared in Fig. 3. It could be observed that the results of the established model are in good agreement with those simulated by ADAMS software, this demonstrates the correctness of the nonlinear coupled motion equations established in section 2.

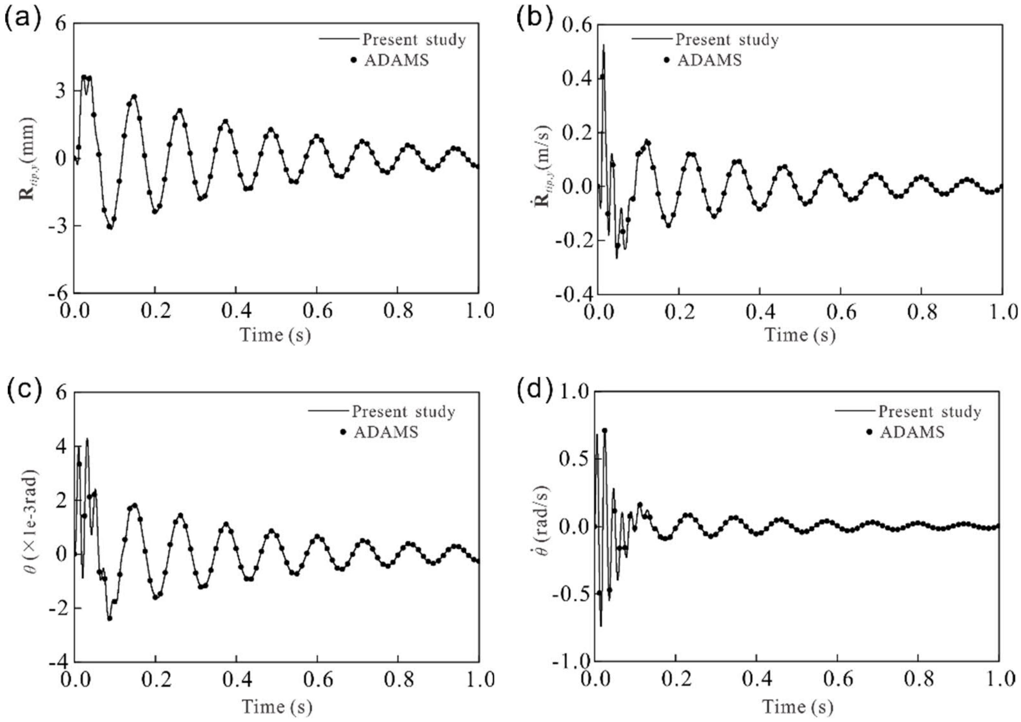

Fig. 3 Model validation by comparing present results with those simulated by ADAMS software: (a) vertical displacement of the beam tip; (b) vertical velocity of the beam tip; (c) angular displacement of the rigid hub; (d) angular velocity of the rigid hub.

3.2. The effect of rotating radius on system dynamics

In following, multi-pulse excitation is applied to the hub, as shown in Fig. 2. The time interval between each pulse excitation is 0.1s. In this subsection, we consider the case of $J=0.1$, $L=0.8$, $c=1.5$, $k=1000$, and let r varies from 0 to 1. The bifurcation diagrams of the system are plotted in Fig. 4 for different values of rotating radius. Fig. 4(a) is the bifurcation diagram of the vertical displacement of the beam's tip. In order to show the bifurcation clearly, $\mathbf{R}_{tip,y}-r$ is computed. Fig. 4(b) is the beam tip deflection in the local coordinate system and Fig. 4(c) is the angular displacement of the rigid hub.

It could be found in Fig. 4(a) and (b) that for the small rotating radius, the beam vibrates periodically, and the corresponding Poincaré section and phase-plane are plotted in Fig. 5 (a), (b). As r increases, the periodic motion of the system disappears gradually. Two typical Poincaré sections and phase-planes are displayed in Fig. 5(c, d) and (e, f), the rotating radius of them are 0.6 and 0.9, respectively.

Comparing Fig. 4(a-c), it could be observed that Fig. 4(a) is similar to Fig. 4(c), this indicates that the periodic motion characteristic of beam's tip is mainly depend on the hub rotation.

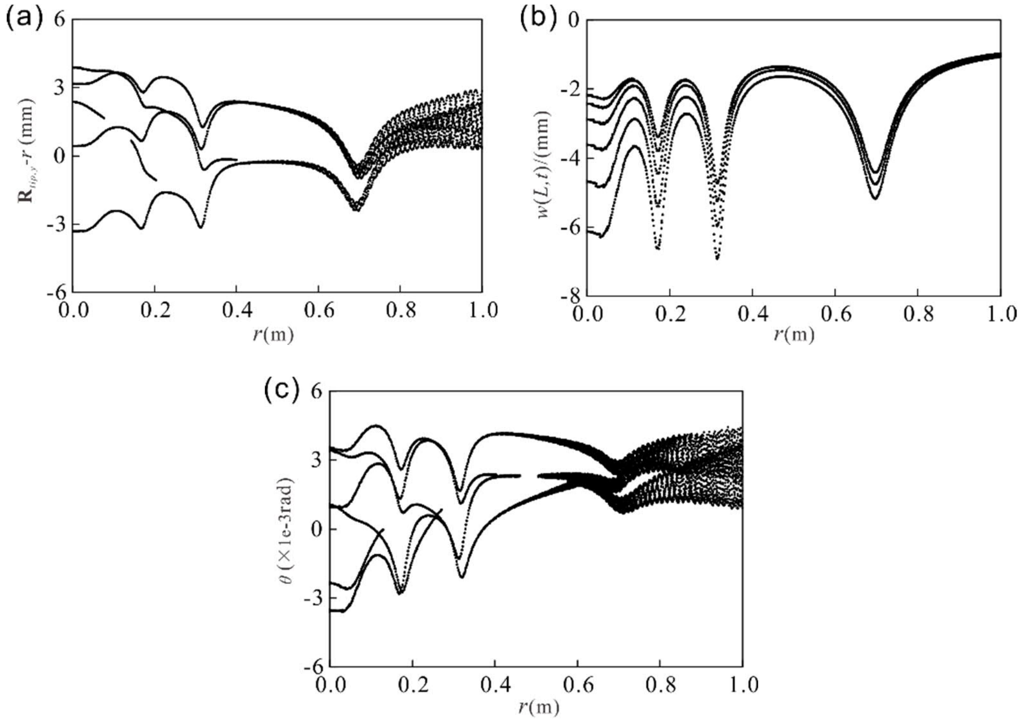

Fig. 4 Bifurcation diagrams as rotating radius is varied: (a) vertical displacement of the beam tip; (b) beam tip deflection in the local coordinate system; (c) the angular displacement of the rigid hub.

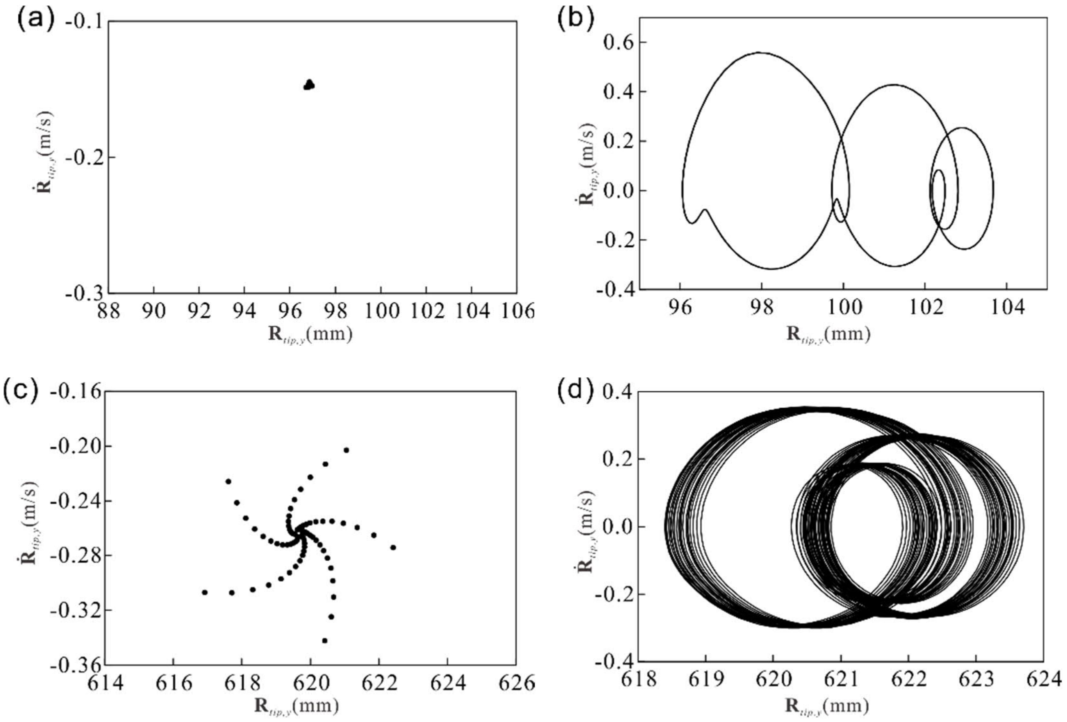

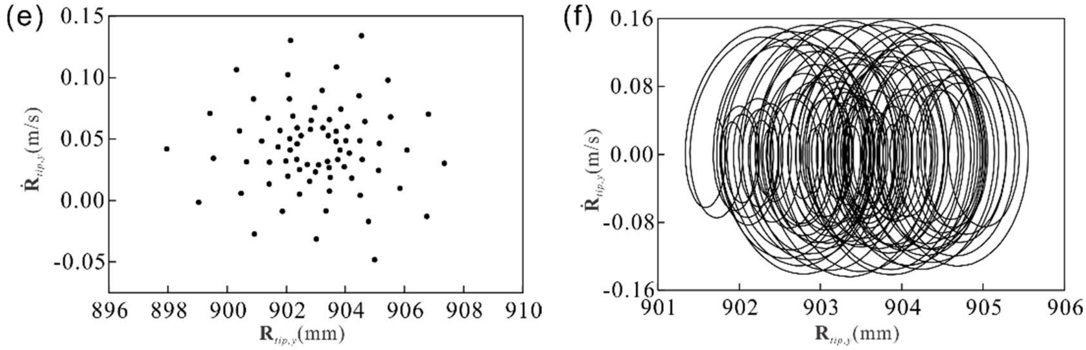

Fig. 5 Poincaré section (a, c, e) and phase-plane (b, d, f) of the system at: (a, b) r =0.1; (c, d) r =0.6; (e, f) r =0.9.

3.3. The effect of beam length on system dynamics

In this subsection, we consider the case of r =0.1, c =0.5, k =1000, and let beam length L vary from 0.5 to 1. The bifurcation diagrams of the system are plotted in Fig. 6 for different values of beam length.

Inspecting Fig. 6(a) and (c), it could be found that for the shorter beam length, its tip has a periodic motion in the vertical direction. Fig. 7(a) and (b) display a typical Poincaré section and phase-plane at L=0.6. As L further increases, the periodic motion of the system disappears gradually, as shown in Fig. 6(b) and (e). Two typical Poincaré sections and phase-planes are displayed in Fig. 7(c, d) and (e, f), the beam length of them is 0.7 and 0.9, respectively. This phenomenon could be attributed to the phenomenon that as beam length increases, the moment of inertia of the system increases. As a result, the torsional stiffness to the moment of inertia ratio decreases.

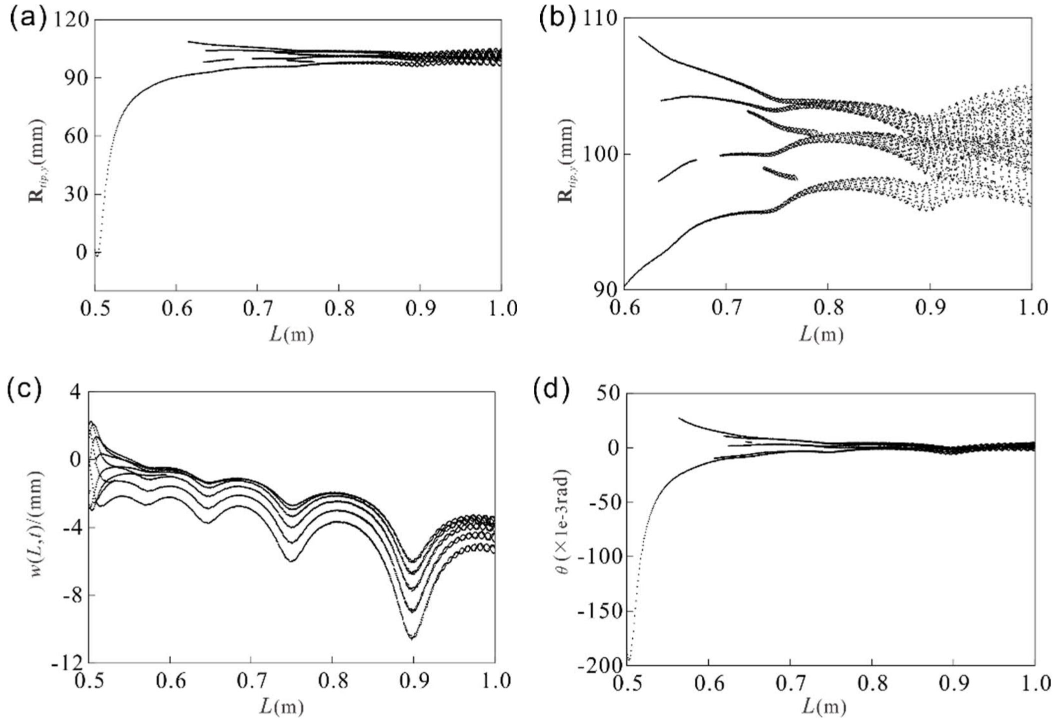

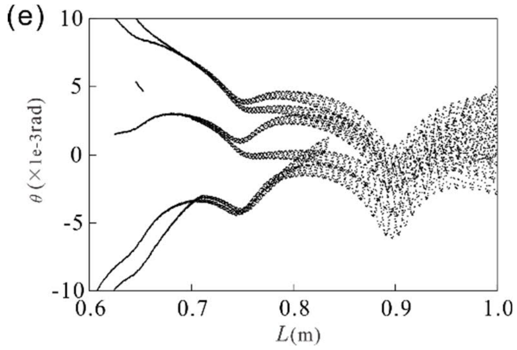

Fig. 6 Bifurcation diagrams as beam length is varied: (a) vertical displacement of the beam tip; (b) magnified plot of (a); (c) beam tip deflection in the local coordinate system; (d) angular displacement of the rigid hub; (e) magnified plot of (d).

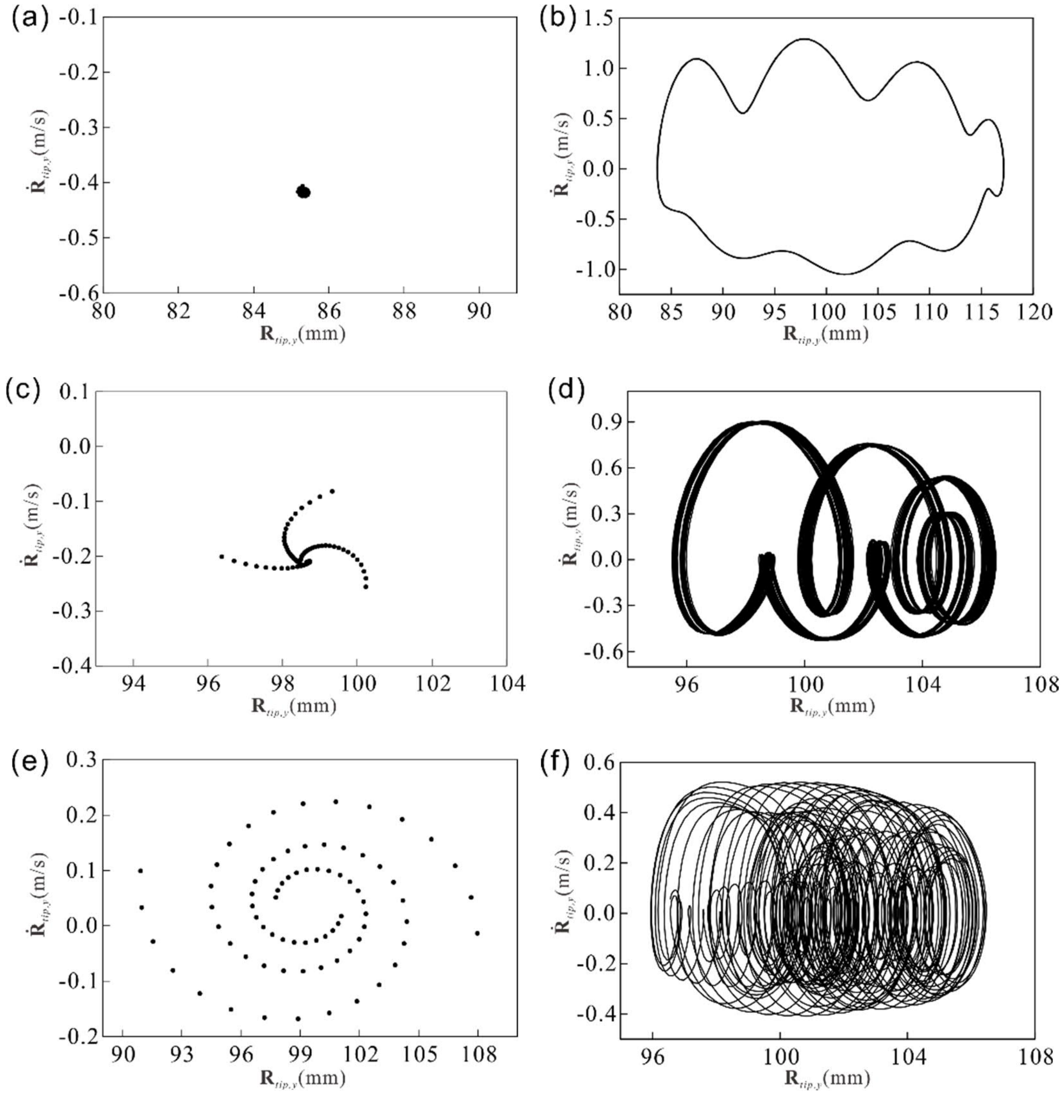

Fig. 7 Poincaré section (a, c, e) and phase-plane (b, d, f) of the system at: (a, b) L =0.1; (c, d) L =0.6; (e, f) L =0.9.

3.4. The effect of torsional stiffness on system dynamics

In this subsection, we consider the case of r =0.1, L =0.8, c =0.5, and let torsional stiffness k varies from 200 to 2000. We plot in Fig. 8 the bifurcation diagrams of the system for different values of torsional stiffness.

It could be observed from Fig. 8(a) and (c) that for the small torsional stiffness, the periodic motion characteristic of rotating beam system is relatively week. The Fig. 9(a) and (b) display a typical Poincaré section and phase-plane at k =240. As the torsional stiffness k increases, the periodic motion characteristic will be enhanced gradually. Two typical Poincaré sections and phase-planes are displayed in Fig. 9(c, d) and (e, f), the torsional stiffness of them are 1180 and 2000, respectively. However, it is interesting to find that as the torsional stiffness increases from 1000 to 2000, no significant improvement of the periodic motion is observed, as depicted in Fig. 8(a) and (c). When k arrives 2000, the motion of the system is still behaving as quasi-periodic, as shown in Fig. 9(e, f). This is because that structural stiffness could not dissipate the vibration energy effectively.

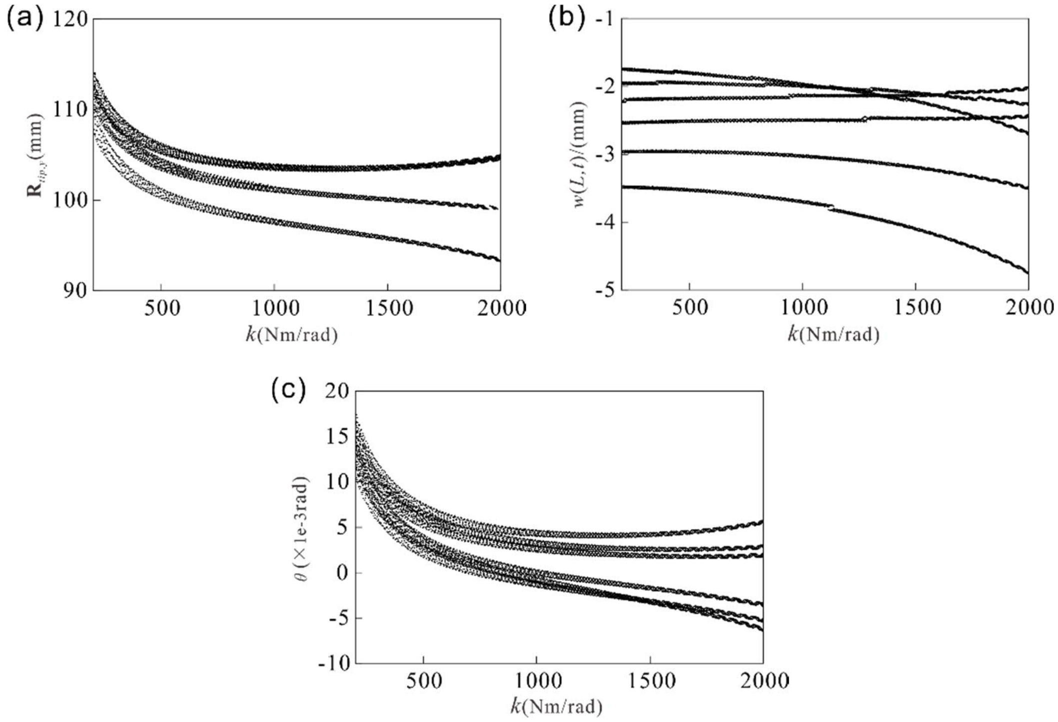

Fig. 8 Bifurcation diagrams as torsional stiffness is varied: (a) vertical displacement of the beam tip; (b) beam tip deflection in the local coordinate system; (c) angular displacement of the rigid hub.

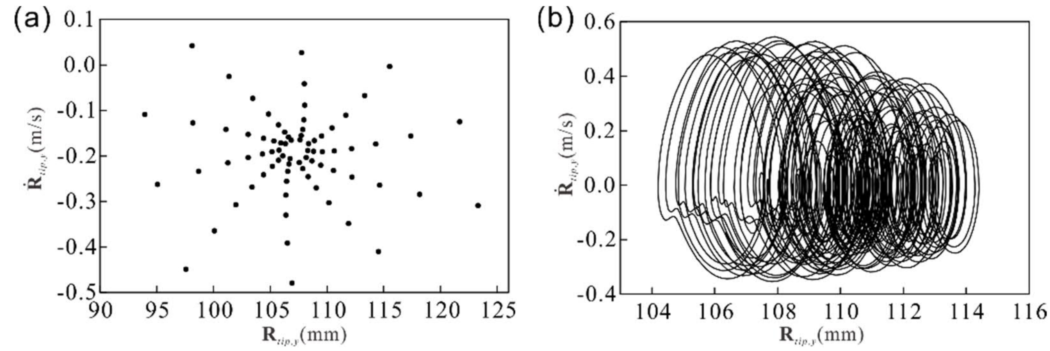

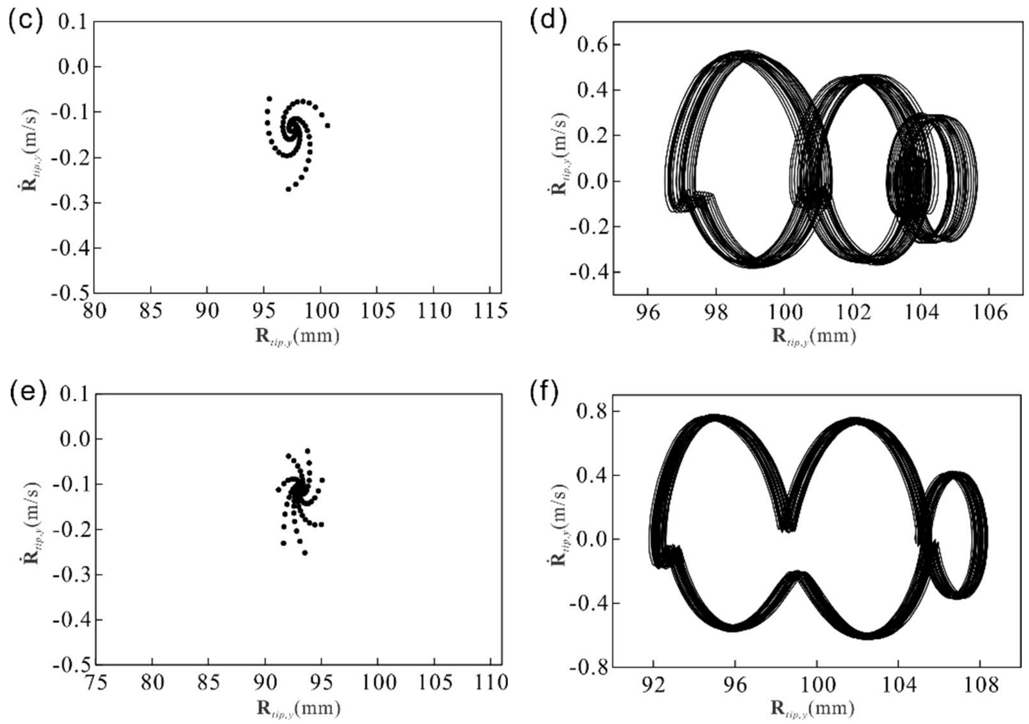

Fig. 9 Poincaré section (a, c, e) and phase-plane (b, d, f) of the system at: (a, b) k =240; (c, d) k =1180; (e, f) k =2000.

3.5. The effect of torsional damping on system dynamics

In this subsection, we vary the torsional damping from 0 to 2, and the other parameter are: r =0.1, L=0.8, k =1000, respectively. The bifurcation diagrams of the system for different values of torsional stiffness are plotted in Fig. 10. Inspecting Fig. 10(a-c) it could be observed that as the torsional damping increases, the motion of the system will become periodic motion, and the critical point is at about c =1. Three typical Poincaré sections and phase-planes are displayed in Fig. 11(a, b), (c, d) and (e, f), the torsional damping of them is 0, 0.5 and 2, respectively.

Comparing section 3.4 and 3.5, it could be observed that increase the torsional stiffness could enhance the periodic motion characteristic of the rotating beam system. However, increasing the tripod stiffness significantly is relatively difficult in practical engineering. Therefore, matching the torsional damping is a feasible approach in this case.

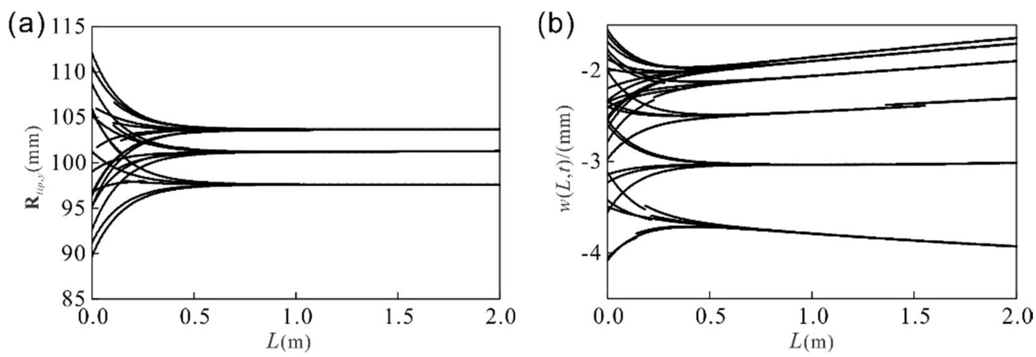

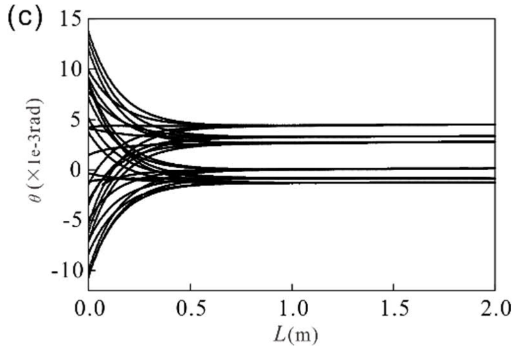

Fig. 10 Bifurcation diagrams as torsional damping is varied: (a) vertical displacement of the beam tip; (b) beam tip deflection in the local coordinate system; (c) angular displacement of the rigid hub.

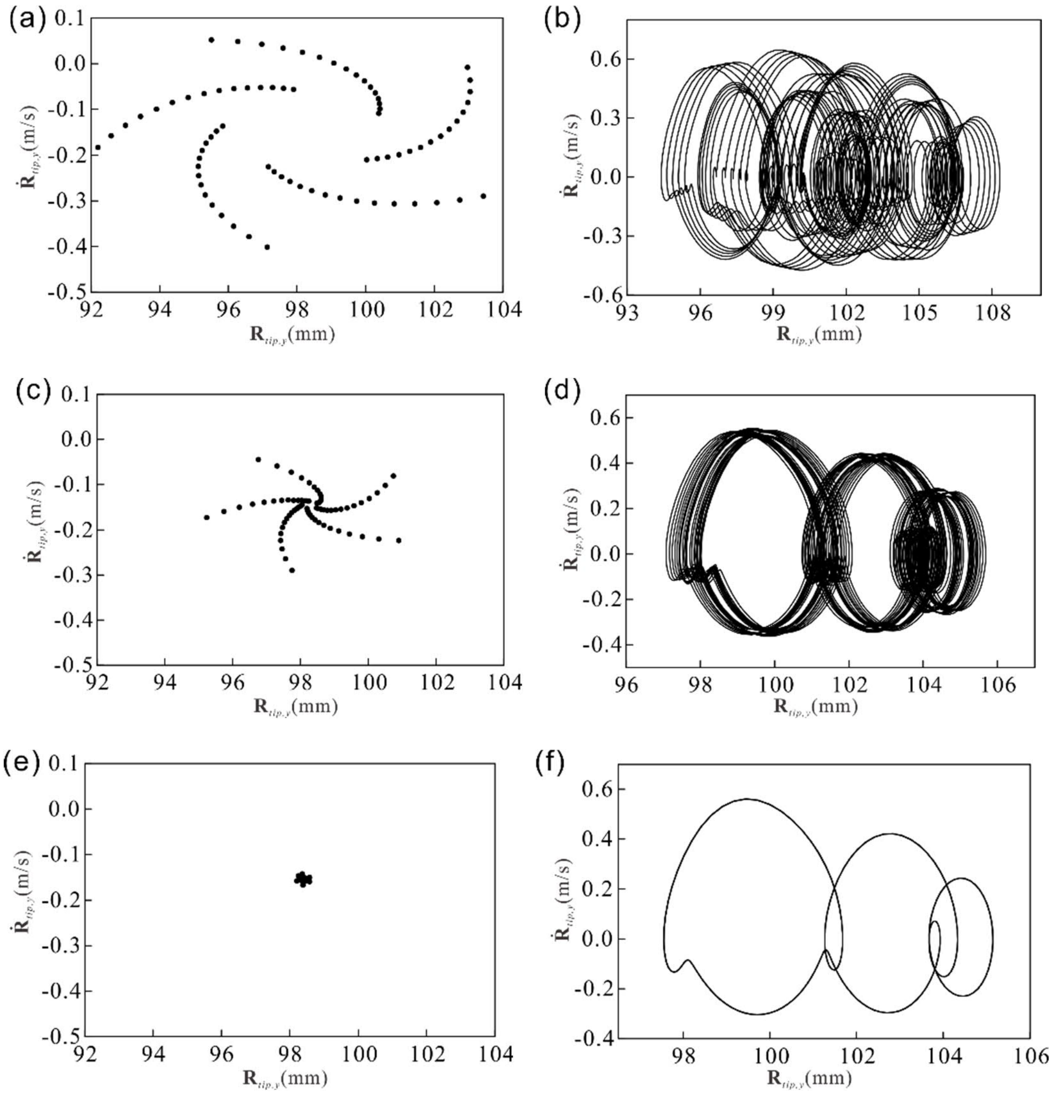

Fig. 11 Poincaré section (a, c, e) and phase-plane (b, d, f) of the system at: (a, b) c =0; (c, d) c =0.5; (e, f) c =2.

4. Conclusions

In this study, a demonstrated machine gun system is simplified as a rotating beam system to study its motion characteristic under a multi-pulsed excitation. Based on the computed responses, the effects of the key structural parameters, including rotating radius, beam length, torsional stiffness and damping on system dynamic behavior are discussed. The conclusions are as follows,

1) Increasing the rotating radius and beam length could affect the periodic motion of the system gradually. As the rotating radius and beam length increase to a certain extent, the motion of the system will become quasi-periodic.

2) It is observed that the hub rotation has significant influence on the periodic motion characteristic of the beam's tip. Increasing the torsional stiffness could enhance the periodic motion characteristic of the rotating beam system.

3) The quasi-periodic motion of the system could be suppressed by matching the torsional damping. As the torsional damping increases and exceeds the critical point, the system will vibrate periodically.

References

1. H.L. Hua, Z.Q. Liao, X.Y. Zhang, The self-excited vibrations of an axially retracting cantilever beam using the Galerkin method with fitted polynomial basis functions, *Journal of Mechanical Science and Technology* **2018**, 32, 29-36.
2. H.L. Hua, Z.Q. Liao, H. Guo, Y.J. Chen, Study on launch dynamics and dispersion accuracy of a machine gun system with supporting structures, *Journal of Ordnance Equipment Engineering* **2022**, 43, 42-7.
3. J. Song, H. Hua, Z. Liao, T. Wang, M. Qiu, Combined Size and Shape Optimization of Structures with DOE,RSM and GA, *Journal of Beijing University of Technology* **2018**, 27, 267-75.
4. H.L. Hua, Z.Q. Liao, ADVA-beam element and its function activation control method, *Chinese Journal of Applied Mechanics* **2021**, 38, 2243-9.
5. H. Hua, Z. Liao, J. Song, Vibration reduction and firing accuracy improvement by natural frequency optimization of a machine gun system, *Journal of Mechanical Science and Technology* **2015**, 29, 3635-43.
6. H.L. Hua, M. Qiu, Z.Q. Liao, Dynamic analysis of an axially moving beam subject to inner pressure using finite element method, *Journal of Mechanical Science and Technology* **2017**, 31, 2663-70.
7. J.W. Lee, J.Y. Lee, An exact transfer matrix expression for bending vibration analysis of a rotating tapered beam, *Applied Mathematical Modelling* **2018**, 53, 167-88.
8. Y. Niu, M. Yao, Q. Wu, Nonlinear vibrations of functionally graded graphene reinforced composite cylindrical panels, *Applied Mathematical Modelling* **2022**, 101, 1-18.
9. J. Warminski, L. Kloda, J. Latalski, A. Mitura, M. Kowalczuk, Nonlinear vibrations and time delay control of an extensible slowly rotating beam, *Nonlinear Dynamics* **2021**, 103, 3255-81.
10. L. Kloda, J. Warminski, Nonlinear longitudinal–bending–twisting vibrations of extensible slowly rotating beam with tip mass, *International Journal of Mechanical Sciences* **2022**, 220, 107153.
11. B. Zhang, H. Ding, L.-Q. Chen, Three to one internal resonances of a pre-deformed rotating beam with quadratic and cubic nonlinearities, *International Journal of Non-Linear Mechanics* **2020**, 126, 103552.
12. A. Nekrasov, A. Khachaturian, Towards the sea wind measurement with the airborne scatterometer having the rotating-beam antenna mounted over fuselage, *Remote Sensing* **2021**, 13, 5165.
13. Y.-Z. Zhao, Y.-J. Chiu, C.-H. Yang, G.-F. Yu, Research on heat-elastic coupled vibration in a rotating rigid disk rotor system, *Journal of Mechanical Science and Technology* **2022**, 36, 1667-78.
14. S. Gantasala, J.-C. Luneno, J.-O. Aidanpää, Investigating how an artificial neural network model can be used to detect added mass on a non-rotating beam using its natural frequencies: A possible application for wind turbine blade ice detection, *Energies* **2017**, 10, 184.
15. J.-H. Park, H.-Y. Park, S.-Y. Jeong, S.-I. Lee, Y.-H. Shin, J.-P. Park, Linear vibration analysis of rotating wind-turbine blade, *Current applied physics* **2010**, 10, S332-S4.
16. L. Li, D. Zhang, W. Zhu, Free vibration analysis of a rotating hub–functionally graded material beam system with the dynamic stiffening effect, *Journal of Sound and Vibration* **2014**, 333, 1526-41.
17. H. Hua, Z. Liao, X. Zhang, Muzzle dynamic characteristics analysis and its matching for firing accuracy improvement, *Journal of Vibration and Shock* **2017**, 36, 29-33.
18. H. Hua, Z. Liao, M. Qiu, J. Li, J. Song, Application of topography optimization in frequency design of machine gun barrel and its efficiency on firing accuracy, *JVE* **2015**, 28, 946-51.
19. H. Hua, Z. Liao, M. Qiu, J. Song, J. Li, Multi-objective optimization combining response surface model of machine gun tripod based on mesh morphing, *Journal of Vibration and Shock* **2015**, 34, 141-6.
20. H. Hua, Z. Liao, J. Song, M. Qiu, J. Xiao, The Application of Reverse Jet Gas Technology in Improving Firing Accuracy of a Machine Gun System, *AcArm* **2015**, 36, 2241-6.

21. H.L. Hua, Study on the Dynamics of Eccentrically Rotating Beam and Axially Moving Cantilever Beam [D]: Nanjing University of Science & Technology; 2018.
22. H. Hua, Z. Liao, X. Zhang, An Efficient Dynamic Modeling Method of An Axially Moving Cantilever Beam and Frequency Response Analysis, *Chinese Journal of Theoretical and Applied Mechanics* **2017**, 49, 1390-8.
23. M. Salehi, P. Sideris, Enhanced Rayleigh damping model for dynamic analysis of inelastic structures, *Journal of Structural Engineering* **2020**, 146, 04020216.
24. J. Li, X. Li, L. Ju, X. Feng, Stabilized integrating factor Runge--Kutta method and unconditional preservation of maximum bound principle, *SIAM Journal on Scientific Computing* **2021**, 43, A1780-A802.